General Macro- and Microphysical Properties of Deep Convective Clouds as Observed by MODIS

TIANLE YUAN* AND ZHANQING LI

Department of Atmospheric and Oceanic Sciences, and Earth System Science Interdisciplinary Center, University of Maryland, College Park, College Park, Maryland

(Manuscript received 12 March 2009, in final form 4 December 2009)

ABSTRACT

Deep convective clouds (DCCs) are an important player in the climate system. In this paper the authors use remote sensing data mainly from the Moderate Resolution Imaging Spectroradiometer (MODIS) cloud product to investigate a few general cloud macro- and microphysical properties of DCCs. This investigation concentrates on the tallest convective clouds and associated thick anvils that are labeled ''deep convective clouds.'' General geographical patterns of DCCs from MODIS data are consistent with previous studies. By examining statistics of optical properties of DCCs over different locations of the globe, it is found that cloud optical depth distribution for DCCs shows little interannual variability for individual regions. These distributions, however, change with geographical regions. DCC ice particle size varies with surface elevation and cloud brightness temperature. DCCs that develop over elevated areas tend to have smaller ice particles at cloud top. There is a positive correlation between ice particle size and brightness temperature. The slope of this correlation has significant regional variations, which can be explained either with a simple thermodynamic consideration or with homogeneous freezing of aerosols. The findings have important implications in studying radiation budget, ice cloud microphysics parameterization, and troposphere–stratosphere water vapor exchange.

1. Introduction

Deep convective clouds (DCCs) are characterized by high vertical reach and relatively small areal coverage. They play an important role in the climate system. Previous studies (Ramanathan et al. 1989; Harrison et al. 1990; Hartmann et al. 1992) using satellite data have shown that net radiative forcing for DCC systems on large scale is close to zero with large negative shortwave (SW) forcing canceling out large positive longwave (LW) forcing. Kiehl (1994) used a simple calculation to explain the cancellation, which results from a coincidence between tropopause temperature that determines outgoing cloud longwave flux and DCC cloud albedo that controls reflected shortwave flux. Further investigation (Hartmann et al. 2001) proposed that DCCs and associated cloud types must be considered as an ensemble to observe the cancellation. Departures from the cancellation are noted in other studies (e.g., Futyan et al. 2004) when the parameters are not averaged over sufficiently large area and/or a long enough period of time. The intricate balance is crucial for climate studies and thus warrants further investigation as to how DCC systems are structured and therefore why they do not produce large net radiative forcing.

Subvisible cirrus clouds are optically thin in the shortwave and strongly absorbing in the longwave. Existing almost everywhere and temporally persistent, especially in the tropics (Liou 1986), they impose a significant large-scale radiative forcing on the atmosphere (Hartmann et al. 1992). These clouds reduce the solar radiation reaching the surface by reflection and strongly absorb infrared (IR) radiation emitted by the earth's surface and lower atmosphere, emitting IR radiation at much colder temperatures. The net radiative effects of these clouds depend on the surface reflectance, cloud height, cloud lifetime, cloud ice water content (IWC) and cloud microphysics (Stephens et al. 1990; Stephens 2005). Microphysical properties of cirrus clouds affect cloud lifetime in

* Current affiliations: Joint Center for Earth Systems Technology, University of Maryland, Baltimore County, Baltimore, and NASA Radiation and Climate Branch, Goddard Space Flight Center, Greenbelt, Maryland.

Corresponding author address: Tianle Yuan, Department of Atmospheric and Oceanic Sciences, University of Maryland, College Park, College Park, MD, 20742.
E-mail: yuan@atmos.umd.edu

DOI: 10.1175/2009JCLI3136.1

the atmosphere because clouds with large ice particles tend to precipitate out and dissipate while those with smaller ice particles may sustain themselves through radiative effects and stay in the air longer (Jensen et al. 1996). These properties are also important in regulating the stratospheric moisture because smaller ice particles are more likely to remain suspended in the air that enters the stratosphere and thus provide more moisture there (Sherwood 2002). DCCs and cirrus clouds are strongly connected as a large amount of ice water mass is detrained from DCC systems as detached anvil clouds. These detached anvil clouds can evolve into cirrus clouds, thus making DCC anvils an important source of cirrus cloud formation (Rossow and Schiffer 1999; Mace et al. 2006 and references therein). Ice microphysics for DCCs therefore has a strong influence on the characteristics and development of cirrus clouds. Improved knowledge of DCC cloud microphysical properties will help to better understand cirrus clouds.

High cloud microphysics parameterization for climate models was pioneered by Heymsfield and Platt (1984) based on in situ measurements of Heymsfield (1975) and lidar measurements of Platt and Dilley (1981) where ice particle size is dependent upon temperature and IWC. The parameterization is crucial for studying cloud feedbacks in the scenario of a global climate change (Platt 1989; Martin et al. 1988) and remains a subject of active research (Donovan 2003; Iacobellis et al. 2003 and references therein). A large difference in model simulated moisture, cloud fraction, and temperature fields as well as radiative budgets can result from different parameterizations. A study by Kristjansson et al. (2000) demonstrated that improved ice particle parameterization could reduce cold bias in the upper troposphere and produce a better longwave radiation budget. Large radiative flux sensitivities are found due to parameterization of ice particle sizes. The difference can be as large as 32 W m^{-2} on the daily time scale and 4 W m^{-2} on the seasonal scale according to Iacoellis et al. (2003). Van Zadelhoff et al. (2007) showed that observation–model difference in terms of radiation flux is reduced from as large as 15 W m^{-2} with an old scheme to 0.7 W m^{-2} using a new parameterization of ice particle sizes (Donovan 2003). They also reported significant changes of yearly average albedo in the model due to parameterization alone. Zurovac-Jevtic and Zhang (2003) modified parameterization schemes in a general circulation model (GCM) and demonstrated the important effect of parameterized ice clouds in terms of cloud fraction and vertical structure as well as moisture exchange between the upper troposphere and tropopause region.

Several parameterizations have been proposed (e.g., Ou and Liou 1995; Ebert and Curry 1992; McFarquhar and Heymsfield 1997; Donovan 2003), most of which are based on in situ and/or active instrument like lidar and radar measurements. Ice crystal effective radius (CER) is assumed to be determined by cloud temperature and/or ice water content or by in-cloud depth from the cloud top. Most of these parameterizations are based on measurements of thin cirrus. Despite being based on a few cases at certain locations, these parameterizations are applied globally regardless of the environment. With the global coverage of remote sensing data it is possible to identify the spatiotemporal variations of ice properties and relationship between CER and temperature. These observations can serve as indicators for future field measurements to verify, which serve as a further step toward better parameterization in our climate models.

In this study we utilize cloud products from the Moderate Resolution Imaging Spectroradiometer (MODIS) to study DCC general macro- and microphysical properties. The purpose of our study is to gain more insight on the cancellation of DCC longwave and shortwave forcing. We put an emphasis on investigating the relationship between MODIS retrieved ice particle size and cloud temperature at the top of DCCs given its application in modeling and understanding of cirrus clouds. We will show that this relationship is geographically dynamic and explain the spatial variation through a simple thermodynamic model.

Datasets employed in this study are summarized in section 2. Methodology and regions of interest are discussed in section 3. Section 4 presents the major findings of our work. Discussions and implications of our results are given in section 5. Section 6 summarizes this study.

2. Data and quantities of interest

The bulk of the data used in this study comes from MODIS level 2 granule cloud products (MOD06 and MYD06; note that the prefixes ''MOD'' and ''MYD'' are used for products based on MODIS measurements onboard of *Terra* and *Aqua* platforms, respectively). In addition, the level 1 subsampled reflectance product (at 5-km resolution) helps us choose individual cases as explained in the methodology section. Channel 31 (11 μm) level 1B 1-km resolution radiance data are used to calculate brightness temperature (BT) as a proxy for cloud vertical reach.

Utilizing the fact that near-infrared reflectance is sensitive to cloud particle size and visible reflectance to cloud water amount, cloud particle size and cloud optical depth (COD) are simultaneously retrieved based on reflected radiation at these two wavelength bands for liquid-phased clouds (King et al. 1992; Platnick et al. 2003). This data

product is validated and/or evaluated by several studies (e.g., King et al. 2004; Mace et al. 2005; Yang et al. 2007). Ice crystal habits complicate the retrieval process applied to ice clouds mainly because of the sensitivity of reflectance to crystal shapes. Better characterization of bulk ice properties is thus critical for improving the quality of retrieved quantities. The latest MODIS product, collection 5, is substantially improved by incorporating more comprehensive crystal habits based on newly available in situ measurements and radiative transfer model calculations (Baum et al. 2005) among other changes as summarized by Yang et al. (2007). Furthermore, the sensitivity of retrieved ice CER to ice crystal habit is alleviated in this study, since DCC optical depths are sufficiently large. Therefore, crystal shape variance should not be as important (Baum et al. 2000). We shall, however, point out the crystal habits used in Baum et al. (2005) are derived from a limited number of in situ measurements. It is also worth noting that CER values used in this study should not be interpreted in an absolute sense but rather as a relative indicator of particle size differences.

Cloud-top pressure (CTP) is retrieved using the so-called CO_2-slicing method. The method utilizes the partial absorption in MODIS infrared bands within the 15-μm CO_2 absorption region (Platnick et al. 2003). Each MODIS band is sensitive to a different atmospheric layer. All three cloud parameters, COD, CER, and CTP, are quality controlled in the MODIS cloud product, and in this study only the highest quality data pixels, as indicated by quality control flags, are used. Brightness temperature, estimated using 11-μm level 1B radiance, serves as a proxy for cloud vertical reach and a crude estimation of the convective strength (Rosenfeld and Lensky 1998).

3. Methodology and regions of interest

a. Data screening

We note that ice cloud properties have significant natural variability in addition to any uncertainties in the remote sensing products. It is necessary to minimize retrieval errors in order to achieve better signal to noise level. The MODIS cloud product has internal flags used for indicating the quality of retrievals that are based on a series of tests as discussed in detail by Platnick et al. (2003). We employ four flags to ensure that each pixel used is at least 99% cloudy, the retrieval is marked as useful and with highest quality, and the cloud phase is ice. Cloud phase is extremely important as water and ice hydrometeors have completely different optical properties (Platnick et al. 2003). Treating water clouds as ice clouds, or vice versa, will inevitably lead to errors in the retrievals, which need to be avoided for our purpose.

b. DCC definition

There is no precise definition of a deep convective cloud using just passive remote sensing measurements. In practice, BT has been used to define DCC by setting a threshold of low BT, T_c (Houze 1989; Sherwood 2002; Liu et al. 2007; Rossow and Schiffer 1999). For different purposes T_c can range from as low as 210 K, to select only the most vigorous convective clouds (Zipser et al. 2006), to as high as 245 K to study the general population of DCC systems (Kubar et al. 2007). Using BT alone cannot differentiate if a cloud is real DCC or a combination of clear-sky and cirrus clouds (Chang and Li 2005). Cloud optical depth is retrieved mainly based on reflected visible solar radiation and is another possible proxy for cloud vertical development. However, for this purpose it suffers from a poor dynamical range, especially when clouds are optically thick like DCCs, since MODIS COD retrievals saturate at 100. We thus combine BT and COD to give us more confidence in selecting cold clouds that are associated with DCCs. We define cloud pixels with BT less than 243 K and COD greater than 40, which further screens out relatively thick, isolated cirrus clouds not associated with an active DCC system but keeps anvils associated with the deep convection. The threshold for BT is chosen to be 243 K because it corresponds to a local minimum in the frequency distribution of MODIS BT, separating low and high clouds (Kubar et al. 2007). We note that the definition used here is not identifying individual convective cells/systems and studying them as in other studies (Roca and Ramanathan 2000; Xu et al. 2005, 2007; Del Genio and Kovari 2002; Futyan and Del Genio 2007).

c. Methodology

Properties of DCCs are extremely dynamic given the wide range of convective strength and a set of extremely complex processes involved. We take advantage of the ample sampling opportunity provided by the MODIS instrument that covers the globe every 2 days. Statistics of cloud properties like CER are derived from the screened dataset for each region to study the gross characteristics of clouds and their geographical variations. Geographical maps are used to investigate their connection with environmental conditions. In addition to studying the natural variability of cloud properties, we want to find physical relationships among cloud properties.

Vertical profiles of ice particle sizes are important in applications of GCM parameterizations (Iacobellis et al. 2003; Van Zadelhoff et al. 2007) and they can lead to large sensitivities in the model as discussed in our introduction. The MODIS cloud product offers retrievals

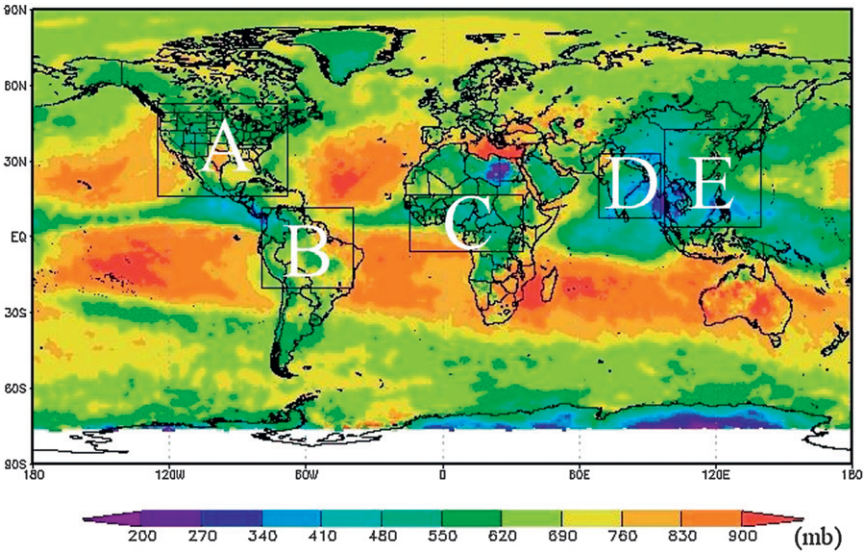

FIG. 1. The global distribution of CTP averaged between June and August 2006 for five study regions: A (North America), B (South America), C (central Africa), D (Indian monsoon), and E (East Asian monsoon) as roughly outlined with five boxes.

CER and BT, from which we can investigate their relationship. We collect simultaneous and collocated measurements of cloud CER and BT during a season for a study area. CERs are averaged into BT bins to construct a CER–BT profile. A profile constructed this way represents the seasonal mean properties of DCCs for a geographic region.

In addition we study the statistics of cloud optical depth and brightness temperature to investigate ensemble structure and organization of DCCs. These statistics of DCC physical properties are important for understanding the radiative forcings by DCCs.

d. Regions of interest

The tropics and extratropical continental areas in summer are active regions for deep convective cloud formation with the tropics being the dominant source (Gettelman et al. 2002; Liu et al. 2007). The regions (Fig. 1) of interest in our study include the southwest Indian monsoon region (region D), including the Indian subcontinent, Bay of Bengal, Arabian Sea, and tropical Indian Ocean; the China and East Asian monsoon region (region E); continental North America (region A); South America (region B); and central Africa (region C). These regions are shown to be active in forming DCCs and they span a wide range of different environmental conditions. Data from eastern Pacific intertropical convergence zone and Pacific warm pool regions are also analyzed. This study will, however, focus on regions A to E.

4. Results

a. Geographical patterns

An example of geographical distribution of the number of DCC occurrence during summer 2002 is displayed in Fig. 2a for the Asian region. The map is made up of 2.5° × 2.5° grid cells and the frequency is calculated as the sum of the number of DCC pixels during the summer over each grid cell. We note again that DCC pixels here are not individual convective cells/systems. Three major areas of active DCC formation are readily identified from the map: the southeast Indian monsoon region (IM), the East Asian monsoon region (EAM), and the Pacific warm pool region (PWP), which are all associated with the large-scale summertime monsoon circulation and high sea surface temperature (Liu et al. 2007). In addition the summertime heating of the Tibetan Plateau (TP) makes it also an active DCC region as indicated by the local maxima in the frequency map (Chen and Liu 2005). For the same reason DCC formations are active over the high plains (not shown here). DCC frequency maps of other study regions like the summertime North America continental region and the South America rain forest region also capture the spatial patterns of convection. Although we are aware of the fact that there are large diurnal variations in DCC formation, the gross spatial pattern seems to be well captured by both the *Terra* and *Aqua* MODIS instruments. For regions like PWP and IM where relatively small diurnal variations exist, we can even treat data from MODIS as representative (Yang and Smith 2006).

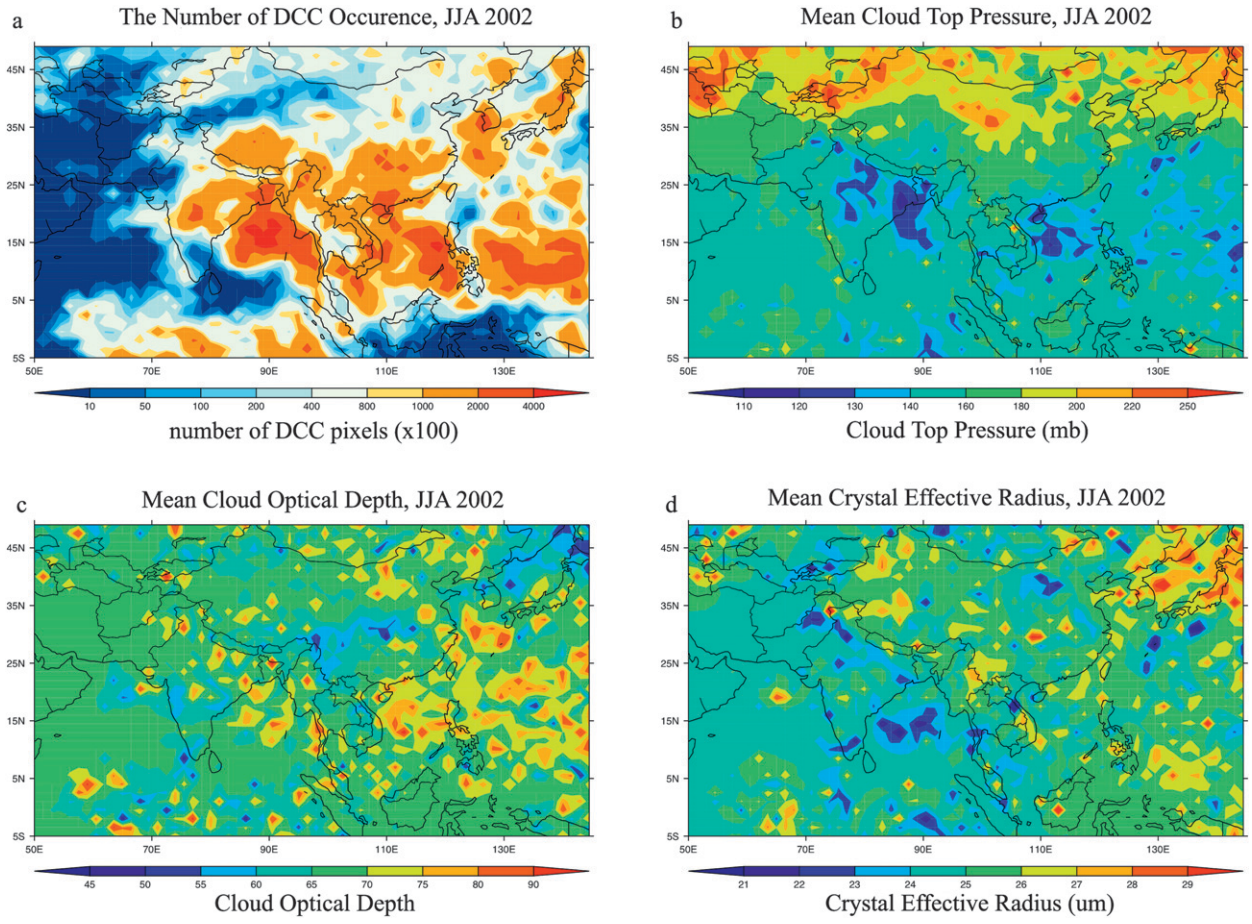

FIG. 2. The distribution of (a) DCC occurring frequency, (b) CTP, (c) COD, and (d) CER for June–August 2002.

The CTP distribution map for the same period is shown in Fig. 2b. The CTP is averaged the same way as frequency data. Generally there is a negative correspondence between the pattern of CTP and the pattern of DCC frequency, indicating active DCC regions on average also produce the deepest clouds in terms of cloud-top pressure. The validity of this correspondence may be limited again by the limited temporal sampling opportunities *Terra* and *Aqua* provide. We will not repeat this limitation again explicitly in later discussions unless it is necessary. There is a general south–north gradient in CTP distribution, in part because of the troposphere-top-height distribution that is higher in the tropics and decreases to the north. According to this map the deepest clouds is found over northern Indian, the South China Sea, and to the south of Japan, where average CTP is between 125 and 100 mb. These clouds probably reach the tropopause region frequently. This is in agreement with previous studies using different radiometers (Zipser et al. 2006). A map of cloud optical depth for the same region and period is shown in Fig. 2c. The COD is generally greater over DCC-active areas like IM, EAM, PWP, and TP. However, an extensive area over northern China has optically thick clouds, but they are of relatively shallow vertical extent as indicated by the high CTP values. This might be due to the high aerosol loading over there, and nucleation of numerous particles is likely to increase optical depth. However, we also note the relatively few DCC samples in this area. Distribution of CER is plotted in Fig. 2d and its pattern is not as well defined as that of frequency or CTP. There is a weak inverse relationship between COD and CER over some areas. Neither CTP nor COD alone would explain the variability of CER and indeed, CER is a microphysical quantity that is under influence of many factors. As discussed later, several important factors have strong influence on CER mean statistics, and simply using and studying data patterns may lead to false conclusions.

b. Physical constraints on CER

In situ and active remote sensing measurements have demonstrated that ice particle sizes for high clouds

strongly depend upon temperature and they are shown to positively correlate with each other (e.g., Heymsfield and Platt 1984), meaning ice particle size increases with temperature, which is opposite to the relationship between droplet size of liquid-phase clouds and brightness temperature (Rosenfeld and Lensky 1998). This positive dependence is postulated to result partly from size sorting (Heymsfield 1975; McFarquhar and Heymsfield 1997).

We apply two methods to examine whether the datasets utilized in our study from passive remote sensing obey the same relationship. In one we compare time series of BT and CER and in the other we examine the relationship between averages of BT and CER. Both methods use data from a fixed region during some time span. An area is selected based on the frequency map to contain significant number of points to increase the statistical robustness. Then time series of areal mean BT and CER is plotted against time for a time period. An example is provided in Fig. 3a. Each point in the plot represents the areal mean for 1 day (x axis). BT positively correlates with CER extremely well, agreeing with the in situ observed relationship (Heymsfield and Platt 1984). CER is plotted against BT in Fig. 3b where BT is divided into equal sample size bins (2 K) and CER is averaged over each bin and this produces a seasonal mean CER profile for an area. The BT–CER profile again shows good agreement with established results, which lends further confidence that the retrievals are physically sound in relative values regardless of their absolute accuracy. This general relationship is observed in our data all over the globe and appears to be universally obeyed although the slope can vary as discussed later.

The influence of cloud-top temperature on CER is universally observed with few exceptions. However, there are several aspects of this relationship that vary geographically, which will be discussed further in later sections. Another source of variations of CER is topography as shown in Fig. 4. Figure 4a shows the geographic distribution of CER from *Aqua* over North America in 2003 and Fig. 4b is a digital elevation map for this region. A pronounced CER minimum is present over the high plains. We propose several environmental conditions that favor smaller ice particle sizes over high elevation areas. From reanalysis data and Atmospheric Infrared Sounder (AIRS) retrievals (map not shown), both total column integrated water vapor (precipitable water) and relative humidity are lower over plateaus as expected. The dry condition increases the cloud-base height for cumulus clouds and therefore lowers cloud-base pressure and temperature. Lower cloud-base pressure and temperature are favorable for activating more droplets because of higher achievable maximum supersaturation level (Johnson 1980). More activated droplets are favorable for

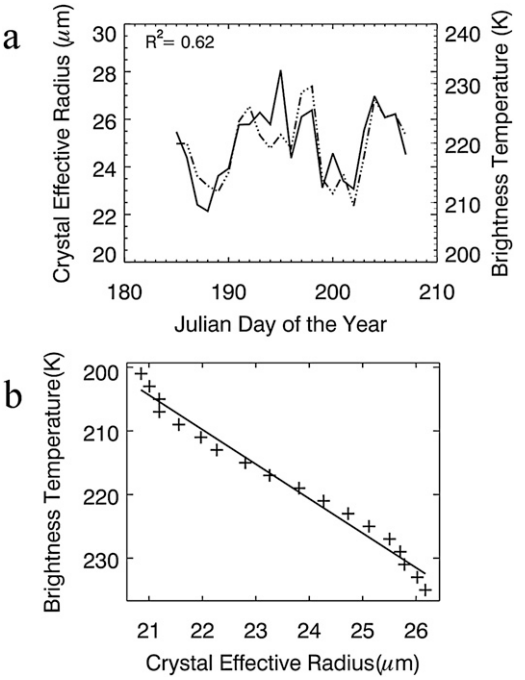

FIG. 3. (a) Time series of cloud brightness temperature and crystal effective radius; (b) a CER–BT profile based on MODIS *Aqua* data over the Amazon basin from 2002. BT is the broken line, and CER is the solid line.

generating smaller droplets and eventually smaller ice crystals. We define in-cloud Lagrangian time T_p as the time it takes for droplets to rise from the cloud base to the homogeneous freezing level (HFL) of −38°C (Rosenfeld and Woodley 2000). To the first order of approximation, we hypothesize that T_p is determined by two major factors: vertical velocity and cloud depth from base to HFL. Low humidity directly contributes to shallower cloud geometric depth by elevating cloud base. The updraft velocity is observed to be usually large inside high plain convective clouds (Houze 1993). These two conditions combine to reduce the time for droplets and ice particles to grow. More activated droplets together with shorter growth time are favorable conditions for generating small ice particles at cloud top. The arguments are summarized in Fig. 5 as a schematic chart. The correspondence between high elevation and small ice particle size can be observed not only in North America but anywhere globally in our dataset. This means that, in addition to cloud height (BT), topography is another important factor that influences ice particle size. There is another possible explanation worth mentioning that concerns pileus clouds generated on top of deep convection. They are made up with extremely small ice particles. However, these clouds are usually optically thin and may not have any impact on MODIS ice retrievals.

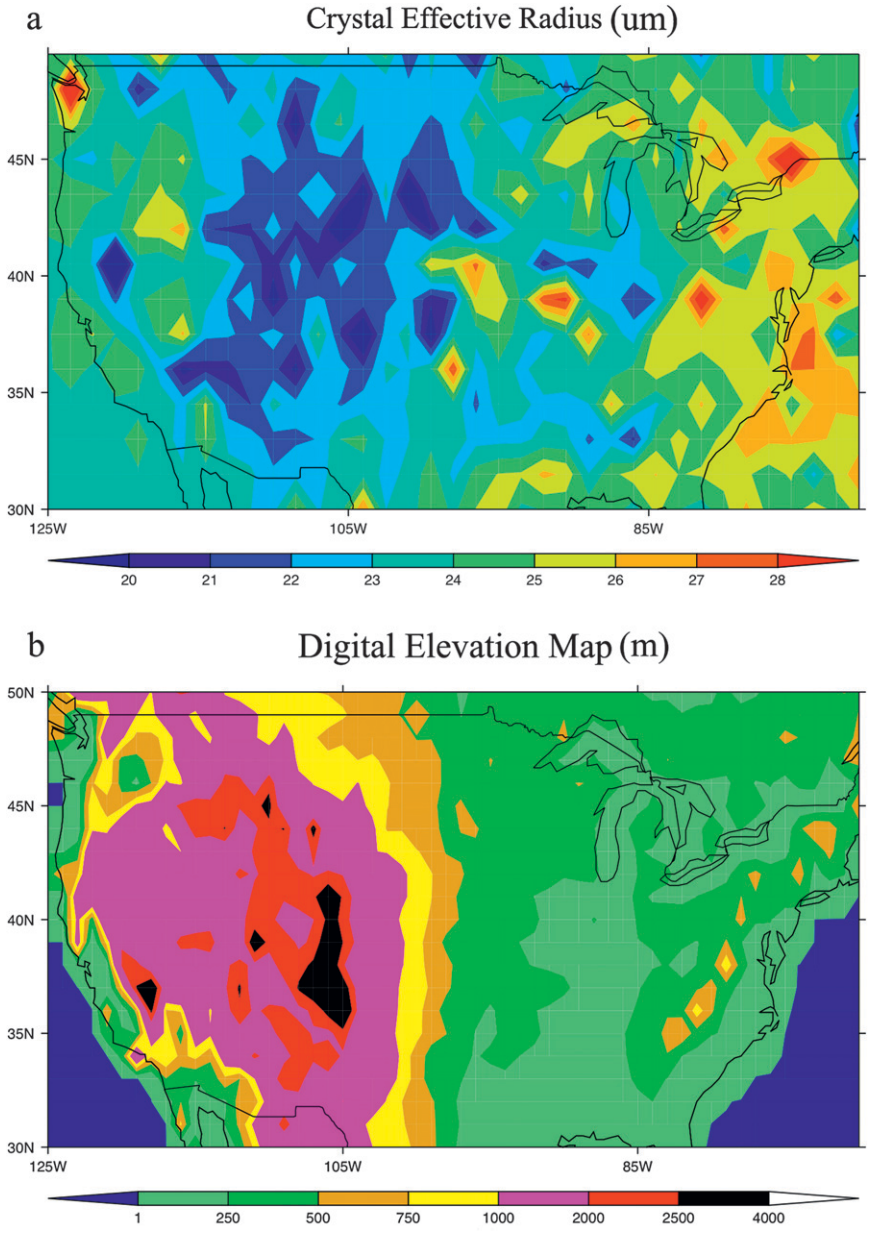

FIG. 4. (a) The distribution of mean CER, and (b) a digital elevation map over the United States.

In addition, we have to assume that pileus clouds occur preferentially over clouds formed over highland areas to explain the observed feature here.

c. *Histograms and cloud structures*

Only a tiny fraction of clouds in nature belong to the deep convective cloud category as defined in our study because cloud occurrence frequency decreases exponentially with decreasing cloud-top BT (Gettelman et al. 2002; Liu et al. 2007). DCCs as defined in this study are estimated to occupy only a few percent or less of the globe depending on what methods and data are used (e.g., Gettelman et al. 2002; Hong et al. 2007; Zipser et al. 2006; Liu et al. 2007; Rossow and Schiffer 1999), and they are made up of convective cores and the thickest part of anvils (Roca and Ramanathan 2000; Kubar et al. 2007). However, these components are key parts of complex convective systems that are important for climate as discussed in the introduction. The structure for this particular set of clouds is worth exploring to get more insight into these processes. For example, the fixed anvil temperature (FAT) hypothesis proposed an

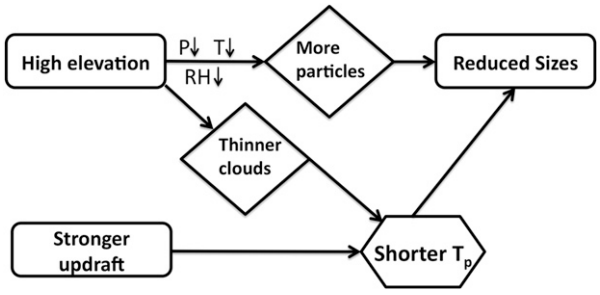

FIG. 5. The schematic diagram of factors and processes favorable for generating small cloud droplets over highland areas and small ice particles.

important constraint on the temperature of DCC anvils resulting from a sharp decrease of clear-sky radiative cooling due to a sharp decrease of water vapor saturation ratio under Clausius–Clapeyron relationship (Hartmann and Larson 2002). Some observational studies (e.g., Xu et al. 2005, 2007) have suggested this hypothesis may hold.

In Fig. 6 DCC BT histograms of the four regions are constructed for both *Terra* and *Aqua* data. Histograms of all regions show a peak around 200 K (except over the Tibetan Plateau, where the convection is not strong enough to penetrate that deep). The distribution is non-Gaussian and is right skewed to low BT. The frequency of extremely cold clouds drops off rapidly once they are colder than the peak as evident by the histograms, which agrees well with previous studies (e.g., Gettelman et al. 2002). We may infer that the peak in BT distributions is attributable to DCC anvils since they are optically thick and spatially dominant. They are formed when convection reaches a constraining stable layer and clouds spread out beneath the stable layer, covering much larger areas than the original convective core. Convective cores only overshoot into the tropopause region over limited areas and thus appear in the BT histograms only in the cold part of the tail. Analyses of individual large DCC systems show a similar structure of DCC BT distributions and therefore support our postulation. From Fig. 6 it is also noted that peak temperature in the distribution, corresponding to the temperature where DCCs detrain their mass and anvils form, has geographical variations that are probably associated with large-scale circulations that determine the temperature of the stable region and therefore the preferential detraining level (Fu et al. 1990; Del Genio and Kovari 2002). The peak temperature also has year-to-year variations for a fixed area, possibly because of local circulation change. Our

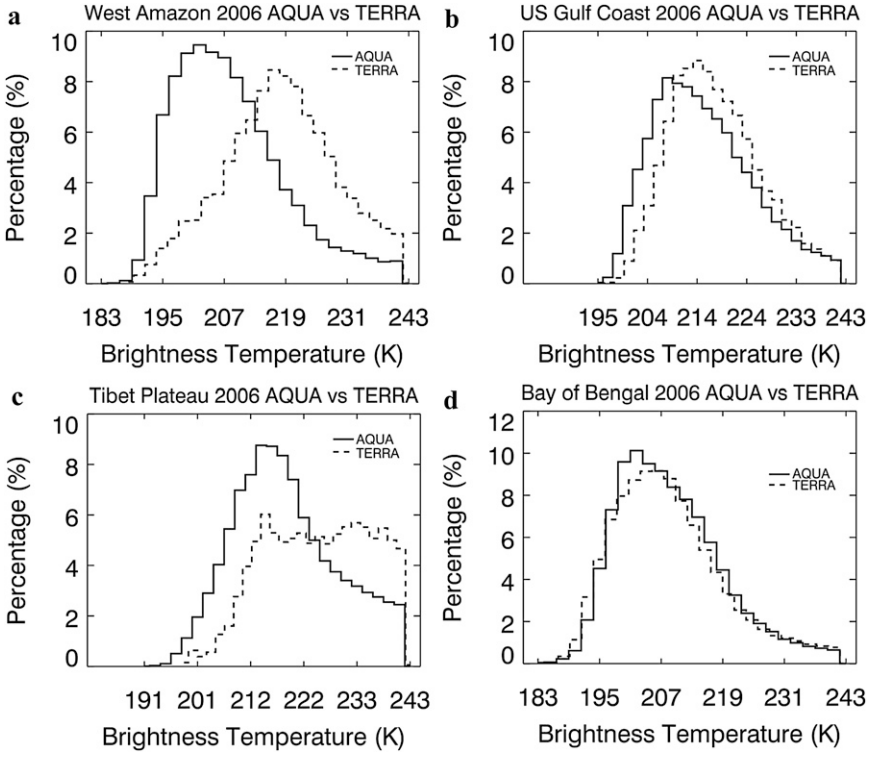

FIG. 6. Histograms of brightness temperature for four regions: (a) the west Amazon, (b) the U.S. gulf coast, (c) the Tibetan Plateau, and (d) the Bay of Bengal.

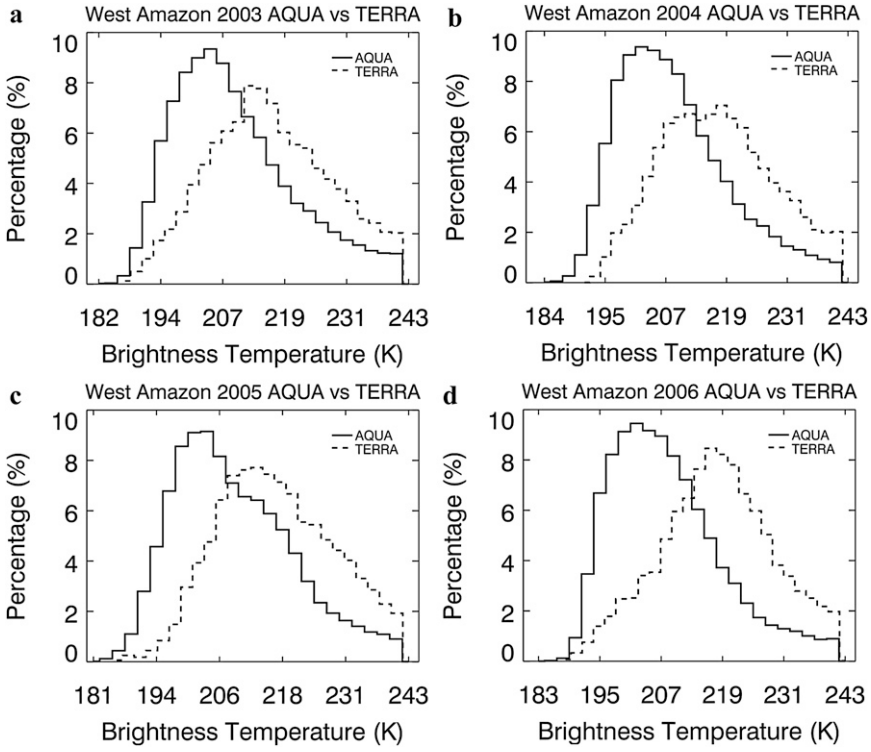

FIG. 7. Histograms of brightness temperature for the west Amazon region.

observations seem to support the FAT hypothesis in that DCCs generally have distribution peaks around 200 K. However, our observations suggest significant variations both geographically and temporally. For a fixed region significant diurnal and annual variations of the detraining level are implied by changes in BT distribution from *Terra* and *Aqua* data as in Fig. 7, which further indicates that detraining levels are not fixed as if they were under a solid lid. We also note there are alternative explanations as to what exactly is the constraint that determines the level of preferred detrainment (Kubar et al. 2007). The difference observed here between *Aqua* and *Terra* is mainly reflecting the diurnal cycle of convection (Yang and Smith 2006). Convections are stronger in the early afternoon as suggested by the colder peak temperature in the *Aqua* data.

We are interested in the balance of longwave and shortwave forcing for DCCs. For this purpose COD is important in regulating shortwave forcing of these clouds in addition to BT's role in regulating outgoing longwave radiation (Rossow and Schiffer 1999; Hartmann et al. 2001; Xu et al. 2005). These two quantities are often used together in radiation models to calculate radiative forcing with additional assumptions (e.g., Hartmann et al. 2001 and references therein). We therefore carry out similar analyses for COD as those of BT. There have been different arguments on whether the near cancellation of LW and SW forcing for tropical DCC active regions is due to DCCs alone or if it is rather due to the distribution of the whole cloud system that includes both DCCs and other shallower clouds accompanying them (Hartmann et al. 2001, and references therein). Only the deepest clouds are included in our study and therefore examination of these clouds will shed light on whether high, thick clouds alone lead to cancellation of LW and SW forcing or the whole spectrum of clouds needs to be considered to have the cancellation.

In Fig. 8 multiyear DCC COD histograms of four regions are presented for *Aqua* data. The peak at the right end of the COD distribution is due to the combination of two factors. One is that MODIS COD product has an upper limit of 100 and the other is that thick anvil clouds cover larger areas as shown in the BT distributions. The peak is especially pronounced for distributions over the tropical regions, which we think is ultimately caused by the structure of individual systems: DCC systems formed in the tropics tend to have larger and thicker anvils associated with convective cores compared to those over the subtropics or high elevation areas. This difference can be clearly seen by comparing two regions that have two extreme distributions: the Bay of Bengal and the Tibetan Plateau. The COD distribution for the Bay of Bengal region peaks strongly at the high end while that of TP shows no sign of peak at high COD values.

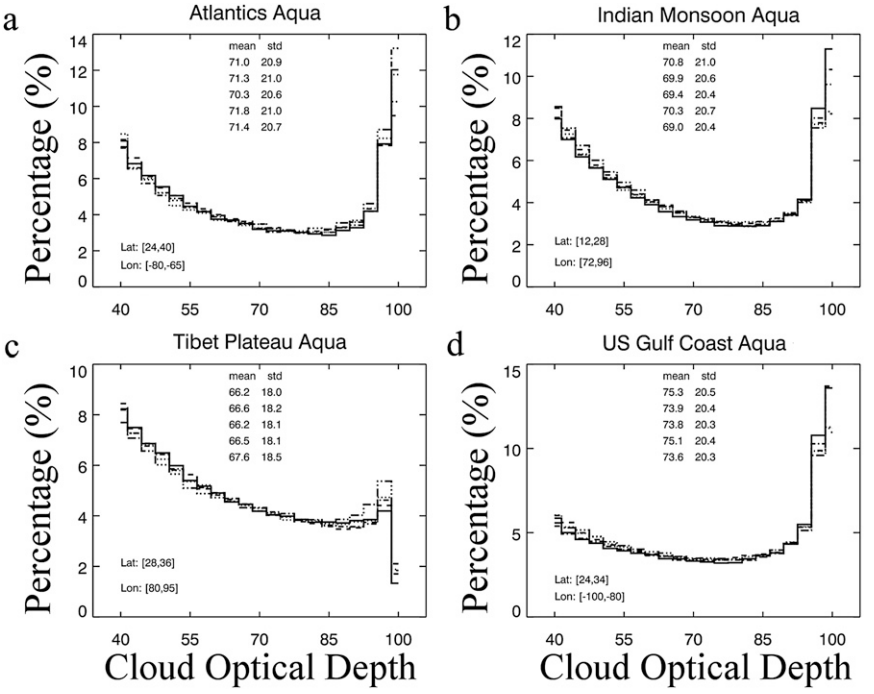

FIG. 8. Distributions of cloud optical depth from *Aqua* in four regions. The mean and standard deviation of the distributions are given for each region indicated by latitude and longitude range in each panel. The means and standard deviations are for the years 2003–2006, and 2002, from top to bottom, in each figure's legend.

We may conceptualize these extremes as two types of DCC organizations: one a mushroom-like structure in the tropics and the other more like turrets over highland areas. As a result of this organization difference, both the means and standard deviations of COD distributions for the tropical DCC systems are generally larger. This structural difference may also be understood in terms of maritime–continental contrast since maritime clouds have more cloud water at the cloud base than continental ones (Futyan and Del Genio 2007). The underlying mechanism for this contrast warrants further investigation.

Furthermore, for individual regions the COD distribution structure is well defined and the shape is extremely stable from year to year as indicated by the almost constant means and standard deviations. The stable statistics of COD distribution for each region suggest that a special kind of organization of DCC systems exists for each region despite yearly variations in local circulations. In other words, DCC systems have local signature structures, at least statistically. Despite the stable local signature structures for individual regions, significant variations are observed not only between regions in the tropics and in the extratropics but also between regions within either tropics or extratropics as suggested in the figure. This geographic variability is in line with findings in previous studies using direct energy flux measurements (Hartmann et al. 2001; Futyan et al. 2004; Futyan and Del Genio 2007) and suggests a strong locality of DCC systems that may be associated with their distinct local environmental conditions. This finding agrees with previous studies that found systematic differences among DCC active regions (Kubar et al. 2007 and references therein). Our results are also in line with systematic difference in cloud morphology found by Mohr and Zipser (1996) using microwave satellite measurements. The mechanisms behind these different organizations warrant further investigation and are beyond the scope of current study.

In Fig. 9 multiyear histograms of four regions using *Terra* COD are presented. We note that, in contrast to the stable statistics of *Aqua* COD data, COD histograms from *Terra* show a different picture. *Terra* and *Aqua* overpass times are in the midmorning and in the early afternoon, which can be crudely used to represent part of diurnal change. Over some regions, DCCs show significant diurnal change (e.g., Yang and Smith 2006 and references therein). The diurnal change can be appreciated by comparing Figs. 8a and 8b. Clouds generally become thicker in the afternoon as indicated by the higher mean values and the real difference between these two is probably greater considering MODIS treats all COD greater than 100 as 100. The shapes of COD distribution are

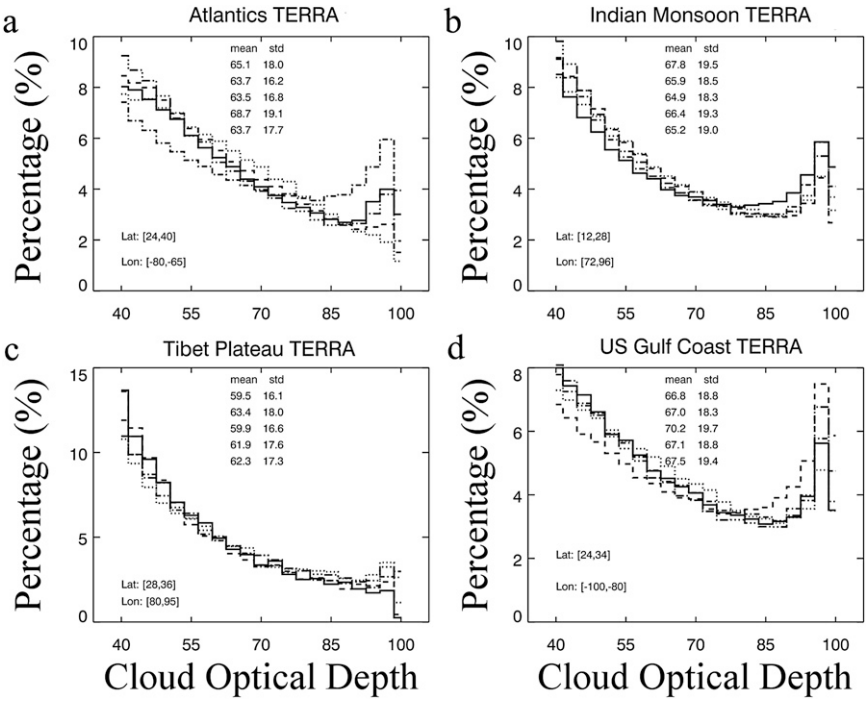

FIG. 9. Same as Fig. 8 except using *Terra* data.

sometimes substantially different in cases like for over the high plains region where a peak in the high CODS end is present only in the afternoon. Although the statistics of *Terra* data still fall within a narrow range, we note significantly larger yearly variations than those of *Aqua* COD histograms are recorded. However, the calibration of MODIS visible channel onboard *Terra* is not as stable as that for *Aqua* (Xiong et al. 2008). Therefore, before this calibration issue is cleared we do not attempt interpret the variation in *Terra* data as being physical.

Based on the distributions of COD and BT we can calculate cloud longwave and shortwave forcing following similar approach in previous studies (e.g., Hartmann et al. 2001 and references therein). Model calculations suggest that for DCC clouds as defined in this study the negative shortwave cloud forcing dominates as shown in Fig. 10. This is simply because of the high shortwave albedo of these thick clouds. For the convective systems to have close to neutral cloud forcing other associated cloud elements need to be taken into account, especially the widespread thin anvil and cirrus clouds, which usually have positive net cloud forcing.

d. Regional variation of CER–BT slopes

An examination of CER–BT profiles over different regions reveals a systematic variation of slopes of CER–BT profiles. The data are confined to BT less than 235 K to insure pure ice clouds because it is already below homogeneous freezing temperature (Rosenfeld and Woodley 2000). In Fig. 11 we show a number of profiles constructed for different areas over the Indian summer monsoon and East Asian summer monsoon regions. Immediately two clusters of profiles can be noticed, one with steeper slopes and the other with slopes distinctly flatter. The first cluster, with slower decreasing rate of CER with cloud-top temperature, is associated with lower-latitude areas like the South China Sea, the Indian Ocean, and the Pacific warm pool. The other cluster is associated with midlatitude areas like central China and the Yellow Sea. Their particle sizes decrease at a faster rate with respect to temperature. Further data restriction is applied to keep only those clouds with BT between 215 and 235 K to have plenty of data points at each BT bin. Four representing large areas are selected to quantitatively assess slope change. These four profiles are shown in Fig. 11. Tropical areas like the Pacific warm pool and the South China Sea have CER–BT slopes of slightly larger than 5 K μm^{-1}, while midlatitude areas such as central China (mean latitude 29°N) and the Yellow Sea (mean latitude 33°N) have slopes of 3.6 and 3.3 K μm^{-1}, respectively.

This latitudinal dependence of the CER–BT profile slope can be also observed over other parts of the globe. An example is given in Fig. 12 where we select four areas sequentially with lower latitude: the eastern United States (mean latitude 28°N), the gulf coast (mean latitude

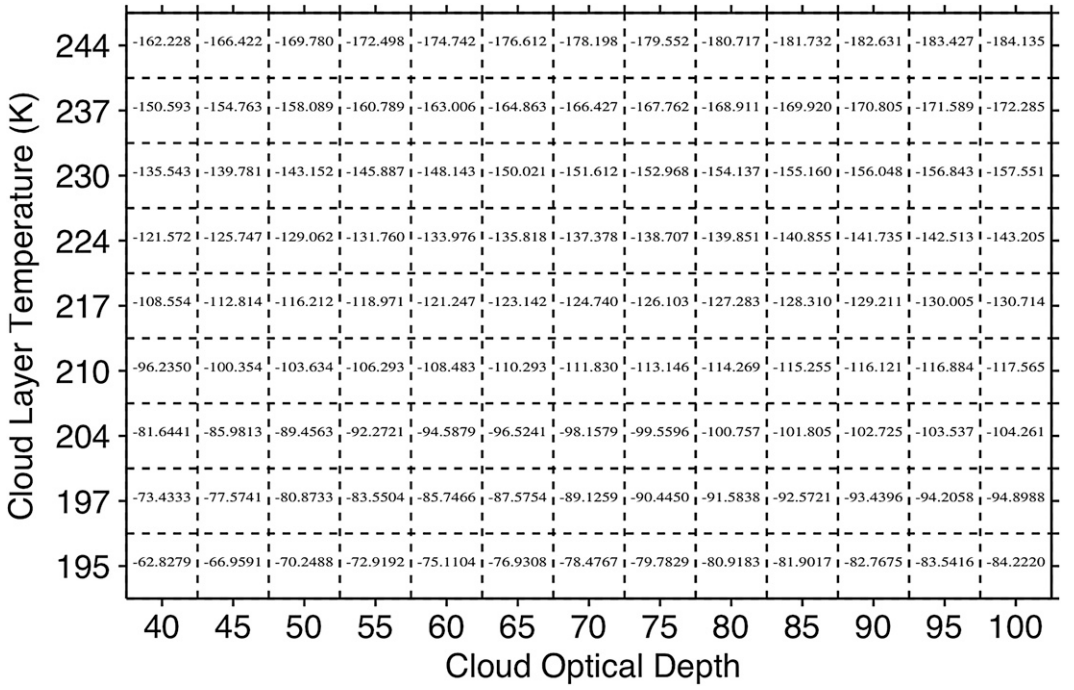

FIG. 10. Cloud forcing diagram calculated for each combination of cloud layer temperature and cloud optical depth as gridded in the figure. The forcing values here are diurnal averages for 15 Jul 2005 over the Indian Ocean (18°N, 84°E).

24°N), the ITCZ region near Central America (mean latitude 8°N), and the tropical Amazon (mean latitude 8°S). The slopes change from approximately 5 K μm^{-1} for the two tropical areas to 3.7 and 3.4 K μm^{-1} for the two midlatitude areas. We include data points that have BT warmer than 210 K and colder than 235 K for enough samples. Slopes for this part of the world are slightly flatter than those of Asian region, although the general decreasing trend of slopes with latitudes holds in both regions.

The slope of CER–BT may be affected by many processes and conditions like entrainment mixing, high-level homogeneous freezing of new particles, updraft velocity, ice crystal habits (Heymsfield et al. 2005), and even satellite retrieval artifacts because of satellite viewing geometry. We can rule out this viewing geometry artifact argument quite effectively by examining data from over the Tibetan Plateau and the high plains. Slopes over these two areas are similar to those observed over the tropics. In addition, this retrieval artifact argument is not in line with the fact that, over the tropics, clouds have different CER–BT relationships depending also on their longitudes. Our data contain no relevant information to other possibilities and thus we have to leave further investigation on these probable causes to future studies when relevant measurements become available.

Here we discuss two likely explanations for the latitudinal variation of CER–BT slopes. First, we attempt to explain part of the variation based on a simple thermodynamic consideration of a parcel experiencing adiabatic ascent whose water vapor is saturated with respect to ice at the beginning. The vertical gradient of the saturation mixing ratio is given by

$$\Gamma_i = \frac{dw_s}{dz}, \tag{1}$$

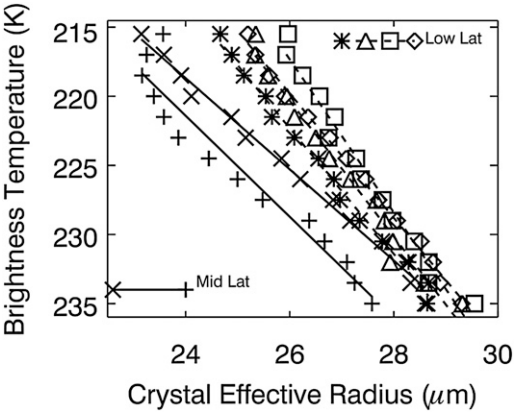

FIG. 11. CER–BT profiles for tropical and midlatitude regions: star [South China Sea (~11°–18°N)], triangle [Indian Ocean (~10°S–0°)], square [warm pool (~11°–18°N)], and diamonds [Indo-Gangetic Plain (~20°–25°N)] are for low-latitude regions; crosses [East China Sea (~30°–36°N)] and pluses [central China (~28°–34°N)] are for two midlatitude regions.

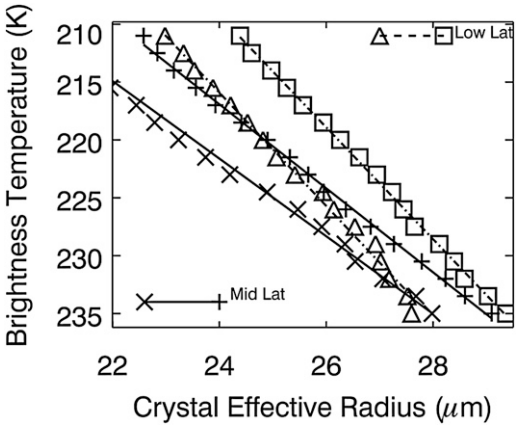

FIG. 12. CER–BT profiles for four areas across the North and South Americas: pluses [eastern United States (~24°–32°N)], triangles [Gulf of Mexico (~32°–36°N)], squares [ITCZ (~4°–12°N)], and crosses [Amazon (~4°–12°S)].

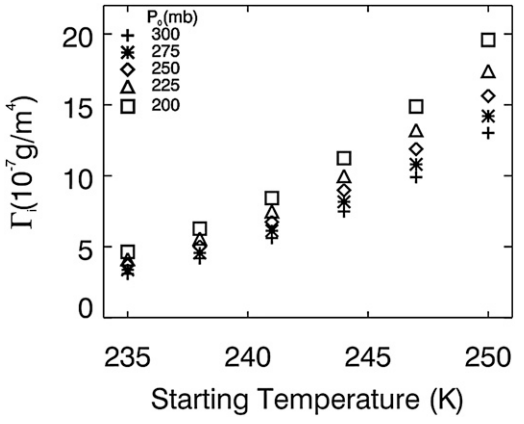

FIG. 13. Ice mixing ratio gradient as a function of air parcel starting temperature and pressure. Different symbols represent different pressures.

where w_s is the ice water mixing ratio calculated as

$$w_s = \frac{\varepsilon e_{si}}{(p - e_{si})}. \tag{2}$$

Here p is the air pressure, e_{si} is the saturation vapor pressure as calculated from Clausius–Clapeyron equation, and $\varepsilon = 0.622$. Following similar steps in Albrecht et al. (1990),

$$\Gamma_i = \frac{(\varepsilon + w_s) w_s l_i}{R_d T^2} \Gamma_{si} - \frac{g w_s p}{(p - e_{si}) R_d T}, \tag{3}$$

where l_i is the latent heat of sublimation, Γ_{si} is the lapse rate if an air parcel follows a moist adiabatic with respect to ice, R_d is the specific gas constant for dry air, and T is temperature. Figure 13 shows Γ_i as a function of parcel temperature and pressure at the starting level. Here Γ_i positively depends upon the temperature at which air parcel starts to ascend. It increases from approximately 5×10^{-7} g m^{-4} to 2×10^{-6} g m^{-4} with temperature increasing from 235 K, the cold end of the freezing level, to 250 K. The Γ_i also has a strong positive dependence on the initial air parcel pressure. An increase of 100 hPa from 200 to 300 hPa at temperature 250 K is accompanied by an increase in Γ_i from approximately 1.3×10^{-6} g m^{-4} to nearly 2×10^{-6} g m^{-4}.

Given the general north–south increase in temperature (in the Northern Hemisphere) and moisture, we know from past studies that cloud base is generally lower in the tropics and thus higher in both temperature and pressure (Williams and Renno 1993; Mace et al. 2007). This is also confirmed by our estimate of lifting condensation level from reanalysis data. Also, because of the geographical distribution of land and ocean, most of the tropical areas with active DCCs are in maritime conditions. Maritime clouds are shown to glaciate at very warm temperatures. The early glaciation means higher glaciation temperature and pressure and therefore larger Γ_i. It can be reasoned that, with other conditions and processes being equal, the decreasing rate of CER with height is slower for parcels with larger Γ_i, which means a higher slope of CER–BT profile. In addition, early freezing creates ice particles that limit homogeneous freezing by consumption of water vapor by deposition growth and possibly at the cost of small droplets (Heymsfield et al. 2005), which further favors slower decreasing rate of CER with height since numerous small droplets may be evaporated because of the lower supersaturation required for larger ice particles and/or accreted by ice particles.

Essentially, this explanation hinges upon the variations of cloud IWC for DCC tops and IWC has systematic latitudinal dependence based on our arguments. A few in situ measurements reported a qualitatively similar relationship between IWC and CER–T (Heymsfield and Platt 1984). In fact, parameterizations based on these in situ measurements indicate the same relationship between IWC and CER–T (Wyser 1998). They show a generally larger IWC for tropical high clouds than midlatitude ones. Further investigations are needed to verify or disprove our explanation.

This explanation of slope variation does not seem to apply for conditions over highland areas. For example, examinations of clouds developed over the high plains and the Tibetan Plateau reveal that slopes for these two areas are closer to maritime conditions. Clearly, other factors need to be taken into account to fully understand the slope variations of CER–BT profiles and we will leave further discussions to later studies.

We propose that one of these factors is the homogeneous freezing of new particles at very cold temperatures. The aerosol loading has a clear contrast between land and ocean and its distribution has a general latitudinal dependence as well (Remer and Kaufman 2006). Numerous aerosol particles coupled with strong updraft inside continental, extratropical, or midlatitude convective clouds are ideal for generation of new ice particles through homogeneous freezing. This new generation of ice particles can significantly reduce the effective particle size. The general contrast between clean, tropical maritime clouds and these continental, polluted clouds thus leads to different slopes of CER–BT through the homogeneous freezing process. We lack detailed information on aerosol size spectra, ice particle concentration, and cloud updraft velocity to make a quantitative assessment on this possibility right now. We shall leave this for future studies when the necessary information is available.

5. Concluding remarks

Using the MODIS cloud products, we investigated deep convective clouds (DCC) of cloud-top brightness temperature less than 243 K and cloud optical depth larger than 40. The general properties are studied over the East Asian monsoon region, the Indian monsoon region, North America, South America, and Africa, during boreal summer. The frequency of DCC occurrence (FDO) is strongly influenced by large-scale circulation pattern except for highland areas, where solar heating of the landmass in the summer generates enough energy to form frequent DCCs. The distribution of the FDO for an ensemble of DCCs is found to be rather stable with little change from year to year but does vary from location to location, especially in different latitude zones. Cloud-top pressure shows a latitudinal dependence, decreasing toward lower latitudes. The detraining height determined by analyzing the distributions of brightness temperature (BT) is found to have a preferential level.

Our analysis on general cloud properties illustrates that seasonally and spatially averaged COD distributions for mature clouds have signature shapes for individual DCC active regions. The distributions of model-generated cloud optical properties may be compared with our observation results. This serves as a reality check for these model parameterizations and could potentially help point to directions for future parameterization efforts. The stable statistics for specific regions suggests that organization of cloud ensembles of specific regions may be governed by certain kind of inherent ''statistical mechanics of clouds.'' Ensemble simulations by cloud-resolving models with representative large-scale forcings for a region can generate ensemble distributions of cloud properties. These simulated ensemble distributions can be analyzed to evaluate a cloud-resolving model's ability to capture the statistical aspect of cloud organization (e.g., Eitzen and Xu 2005; Luo et al. 2007). The so-called superparameterization for general circulation models (GCMs) embeds a cloud-resolving model in each GCM grid (Grabowski 2001; Khairoutdinov and Randall 2001). Statistics of cloud properties from simulations of GCMs with superparameterization could be used to compare with our observation. In addition, significant geographical variations of statistical properties of DCC observed in our study are useful to investigate the performance of ensemble simulations of cloud-resolving models with different local large-scale forcing.

The stable distributions of DCC COD and relatively little variation in BT distributions suggest a relative constant cloud forcing for cloud elements defined in this study. Our calculation suggests that this cloud forcing is negative. Because DCC systems as a whole are almost radiatively neutral (Ramanathan et al. 1989), we infer that other elements of the DCC systems must be included in the consideration and they must also have statistically stable organizations in an ensemble sense to support the observed neutral DCC forcing. We therefore postulate that the DCC systems are made up of a hierarchy of components with stable statistics. Different components interact with each other through radiative and dynamical processes. The interaction among these components may be strongly associated with local environmental conditions. Detailed analysis on these other components of DCC systems is needed to completely understand interactions among these components and their relation to general environmental conditions, as was done for two regions over the Pacific: the east Pacific warm pool and the west Pacific warm pool (Kubar et al. 2007).

The finding of a general relation between the crystal effective radius (CER) and brightness temperature can be explained by size sorting and dependence of water vapor on temperature. The slope of the CER–BT profile is shown to have systematic geographic variations, especially with latitude, steeper in the tropics than the midlatitudes. A simple thermodynamic argument is used to explain part of the slope variation. Temperature and humidity and cloud freezing height are the major factors that affect the slopes. Another important consideration is homogeneous freezing of new ice particles. Other factors like updraft velocity and entrainment conditions need to be taken into account to fully explain the variations.

Although in this study we are looking at DCCs instead of layered high clouds, up to 50% of these layered clouds have their origin in DCCs (Massie et al. 2002; Mace et al.

2005). The results here should be relevant for the issue of high cloud parameterization. The parameterization of high cloud properties is usually a fixed relationship among temperature, ice water content, and ice particle size. Our observations, however, suggest the relationship between temperature and ice particle size has significant variations (McFarquhar and Heymsfield 1997). The variation over relatively lowland areas and ocean can be attributed to basic environmental conditions like relative humidity and temperature that determine cloud base and freezing level. There seems to be an association between intrinsic microphysics with local climate conditions, which leads to the observed regional variation in BT–CER profiles. The variations may also be associated with aerosol loadings. In any case, the variation is at odds with the fixed relationships used in current climate models. It thus warrants further detailed in situ measurements to validate our observations. If in situ measurements agree with our finding, changes to the model parameterization and further understanding of the underlying physics are warranted. The changes could have important radiative consequences (Kristjansson et al. 2000; Van Zadelhoff et al. 2007) and affect the feedback processes of the climate system.

The decrease of CER with height also has an implication in troposphere–stratosphere exchange. Sherwood (2002) demonstrated that smaller ice particle size is favorable for troposphere–stratosphere water vapor transport and is vital to explain the moistening of stratosphere in recent decades. The finding of small ice particle size together with low CTP and high frequency of DCCs over the Tibetan Plateau and the high plains suggest that conditions over these highland regions are active in exchanging water mass between troposphere and stratosphere in the form of ice particles. It has been hypothesized that active and strong convection over the Tibetan Plateau may be one major route for transporting water vapor from troposphere to stratosphere (Fu et al. 2006), and our results seem to support this hypothesis. These conditions are also favorable for generating cirrus clouds from DCC anvils that can last longer given smaller ice particle sizes over the region. These special conditions associated with the high elevation areas in the summer may help to understand how nature regulates cirrus cloud properties and modulates troposphere–stratosphere exchange.

Acknowledgments. We thank Lorraine Remer for her helpful discussion and editing efforts for this work. We also thank Steve Platnick, David O. Starr, J. Vanderlei Martins, Zhibo Zhang, and Xiaowen Li for valuable discussions. This research was supported by research grants from NASA (NNX08AH71G), NASA Interdisciplinary Research in Earth Science (NNH06ZDA001N-IDS), and DOE (DEFG0208ER64571). Finally, we thank the anonymous reviewers for helpful comments.

REFERENCES

Albrecht, B. A., C. W. Fairall, D. W. Thomson, A. B. White, J. B. Snider, and W. H. Schubert, 1990: Surface-based remote sensing of the observed and the adiabatic liquid water content of stratocumulus clouds. *Geophys. Res. Lett.,* **17,** 89–92.

Baum, B. A., D. P. Kratz, P. Yang, S. C. Ou, Y. X. Hu, P. F. Soulen, and S. C. Tsay, 2000: Remote sensing of cloud properties using MODIS airborne simulator imagery during SUCCESS 1. Data and models. *J. Geophys. Res.,* **105** (D9), 11 767–11 780.

——, A. J. Heymsfield, P. Yang, and S. T. Bedka, 2005: Bulk scattering properties for the remote sensing of ice clouds. Part I: Microphysical data and models. *J. Appl. Meteor.,* **44,** 1885–1895.

Chang, F. L., and Z. Li, 2005: A new method for detection of cirrus overlapping water clouds and determination of their optical properties. *J. Atmos. Sci.,* **62,** 3993–4009.

Chen, B., and X. Liu, 2005: Seasonal migration of cirrus clouds over the Asian monsoon regions and the Tibetan Plateau measured from MODIS/Terra. *Geophys. Res. Lett.,* **32,** L01804, doi:10.1029/2004GL020868.

Del Genio, A. D., and W. Kovari, 2002: Climatic properties of tropical precipitating convection under varying environmental conditions. *J. Climate,* **15,** 2597–2615.

Donovan, D. P., 2003: Ice-cloud effective particle size parameterization based on combined lidar, radar reflectivity, and mean Doppler velocity measurements. *J. Geophys. Res.,* **108,** 4573, doi:10.1029/2003JD003469.

Ebert, E. E., and J. A. Curry, 1992: A parameterization of ice cloud optical properties for climate models. *J. Geophys. Res.,* **97** (D4), 3831–3836.

Eitzen, Z. A., and K.-M. Xu, 2005: A statistical comparison of deep convective cloud objects observed by an Earth Observing System satellite and simulated by a cloud-resolving model. *J. Geophys. Res.,* **110,** D15S14, doi:10.1029/2004JD005086.

Fu, R., A. D. Delgenio, and W. B. Rossow, 1990: Behavior of deep convective clouds in the tropical pacific deduced from ISCCP radiances. *J. Climate,* **3,** 1129–1152.

——, and Coauthors, 2006: Short circuit of water vapor and polluted air to the global stratosphere by convective transport over the Tibetan Plateau. *Proc. Natl. Acad. Sci. USA,* **103,** 5664–5669.

Futyan, J. M., and A. D. Del Genio, 2007: Deep convective system evolution over Africa and the tropical Atlantic. *J. Climate,* **20,** 5041–5060.

——, J. E. Russell, and J. E. Harries, 2004: Cloud radiative forcing in Pacific, African, and Atlantic tropical convective regions. *J. Climate,* **17,** 3192–3202.

Gettelman, A., M. L. Salby, and F. Sassi, 2002: The distribution and influence of convection in the tropical tropopause region. *J. Geophys. Res.,* **107,** 4080, doi:10.1029/2001JD001048.

Grabowski, W. W., 2001: Coupling cloud processes with the large-scale dynamics using the Cloud-Resolving Convection Parameterization (CRCP). *J. Atmos. Sci.,* **58,** 978–997.

Harrison, E. F., P. Minnis, B. R. Barkstrom, V. Ramanathan, R. D. Cess, and G. G. Gibson, 1990: Seasonal-variation of cloud radiative forcing derived from the Earth Radiation Budget Experiment. *J. Geophys. Res.,* **95** (D11), 18 687–18 703.

Hartmann, D. L., and K. Larson, 2002: An important constraint on tropical cloud–climate feedback. *Geophys. Res. Lett.,* **29,** 1951, doi:10.1029/2002GL015835.

——, M. E. Ockertbell, and M. L. Michelsen, 1992: The effect of cloud type on earths energy–balance: Global analysis. *J. Climate,* **5,** 1281–1304.

——, L. A. Moy, and Q. Fu, 2001: Tropical convection and the energy balance at the top of the atmosphere. *J. Climate,* **14,** 4495–4511.

Heymsfield, A., 1975: Cirrus uncinus generating cells and evolution of cirriform clouds. Part I: Aircraft observations of growth of ice phase. *J. Atmos. Sci.,* **32,** 799–808.

——, and C. M. R. Platt, 1984: A parameterization of the particle-size spectrum of ice clouds in terms of the ambient temperature and the ice water content. *J. Atmos. Sci.,* **41,** 846–855.

——, L. M. Miloshevich, C. Schmitt, A. Bansemer, C. Twohy, M. R. Poellot, A. Fridlind, and H. Gerber, 2005: Homogeneous ice nucleation in subtropical and tropical convection and its influence on cirrus anvil microphysics. *J. Atmos. Sci.,* **62,** 41–64.

Hong, G., P. Yang, B. Gao, B. A. Baum, Y. X. Hu, M. D. King, and S. Platnick, 2007: High cloud properties from three years of MODIS *Terra* and *Aqua* collection-4 data over the tropics. *J. Appl. Meteor. Climatol.,* **46,** 1840–1856.

Houze, R. A., Jr., 1989: Observed structure of mesoscale convective systems and implications for large-scale heating. *Quart. J. Roy. Meteor. Soc.,* **115,** 425–461.

——, 1993: *Cloud Dynamics*. Academic Press, 573 pp.

Iacobellis, S. F., G. M. McFarquhar, D. L. Mitchell, and R. C. J. Somerville, 2003: The sensitivity of radiative fluxes to parameterized cloud microphysics. *J. Climate,* **16,** 2979–2996.

Jensen, E. J., O. B. Toon, H. B. Selkirk, J. D. Spinhirne, and M. R. Schoeberl, 1996: On the formation and persistence of subvisible cirrus clouds near the tropical tropopause. *J. Geophys. Res.,* **101** (D16), 21 361–21 375.

Johnson, D. B., 1980: The influence of cloud-base temperature and pressure on droplet concentration. *J. Atmos. Sci.,* **37,** 2079–2085.

Khairoutdinov, M. F., and D. A. Randall, 2001: A cloud resolving model as a cloud parameterization in the NCAR Community Climate System Model: Preliminary results. *Geophys. Res. Lett.,* **28,** 3617–3620.

Kiehl, J. T., 1994: On the observed near cancellation between longwave and shortwave cloud forcing in tropical regions. *J. Climate,* **7,** 559–565.

King, M. D., Y. J. Kaufman, W. P. Menzel, and D. Tanré, 1992: Remote sensing of cloud, aerosol and water vapor properties from the Moderate Resolution Imaging Spectrometer (MODIS). *IEEE Trans. Geosci. Remote Sens.,* **30,** 2–27.

——, S. Platnick, P. Yang, G. T. Arnold, M. A. Gray, J. C. Riedi, S. A. Ackerman, and K. N. Liou, 2004: Remote sensing of liquid water and ice cloud optical thickness and effective radius in the Arctic: Application of airborne multispectral MAS data. *J. Atmos. Oceanic Technol.,* **21,** 857–875.

Kristjansson, J. E., J. M. Edwards, and D. L. Mitchell, 2000: Impact of a new scheme for optical properties of ice crystals on climates of two GCMs. *J. Geophys. Res.,* **105** (D8), 10 063–10 079.

Kubar, T. L., D. L. Hartmann, and R. Wood, 2007: Radiative and convective driving of tropical high clouds. *J. Climate,* **20,** 5510–5526.

Liou, K.-N., 1986: Influence of cirrus clouds on weather and climate processes: A global perspective. *Mon. Wea. Rev.,* **114,** 1167–1199.

Liu, C. T., E. J. Zipser, and S. W. Nesbitt, 2007: Global distribution of tropical deep convection: Different perspectives from TRMM infrared and radar data. *J. Climate,* **20,** 489–503.

Luo, Y., K.-M. Xu, Z. A. Eitzen, and T. Wong, 2007: Statistical analyses of satellite cloud object data from CERES. Part III: Comparison with cloud-resolving model simulation of tropical convective clouds. *J. Atmos. Sci.,* **64,** 762–785.

Mace, G. G., Y. Y. Zhang, S. Platnick, M. D. King, P. Minnis, and P. Yang, 2005: Evaluation of cirrus cloud properties derived from MODIS data using cloud properties derived from ground-based observations collected at the ARM SGP site. *J. Appl. Meteor.,* **44,** 221–240.

——, M. Deng, B. Soden, and E. Zipser, 2006: Association of tropical cirrus in the 10–15-km layer with deep convective sources: An observational study combining millimeter radar data and satellite-derived trajectories. *J. Atmos. Sci.,* **63,** 480–503.

——, R. Marchand, Q. Zhang, and G. Stephens, 2007: Global hydrometeor occurrence as observed by CloudSat: Initial observations from summer 2006. *Geophys. Res. Lett.,* **34,** L09808, doi:10.1029/2006GL029017.

Martin, C., C. M. R. Platt, and Harshvardhan, 1988: Temperature-dependence of cirrus extinction—Implications for climate feedback. *J. Geophys. Res.,* **93** (D9), 11 051–11 058.

Massie, S., A. Gettelman, W. Randel, and D. Baumgardner, 2002: Distribution of tropical cirrus in relation to convection. *J. Geophys. Res.,* **107,** 4591, doi:10.1029/2001JD001293.

McFarquhar, G. M., and A. J. Heymsfield, 1997: Parameterization of tropical cirrus ice crystal size distributions and implications for radiative transfer: Results from CEPEX. *J. Atmos. Sci.,* **54,** 2187–2200.

Mohr, K. I., and E. J. Zipser, 1996: Mesoscale convective systems defined by their 85-GHz ice scattering signature: Size and intensity comparison over tropical oceans and continents. *Mon. Wea. Rev.,* **124,** 2417–2437.

Ou, S. C., and K. N. Liou, 1995: Ice microphysics and climatic temperature feedback. *Atmos. Res.,* **35,** 127–138.

Platnick, S., M. D. King, S. A. Ackerman, W. P. Menzel, B. A. Baum, J. C. Riedi, and R. A. Frey, 2003: The MODIS cloud products: Algorithms and examples from Terra. *IEEE Trans. Geosci. Remote Sens.,* **41,** 459–473.

Platt, C. M. R., 1989: The role of cloud microphysics in high-cloud feedback effects on climate change. *Nature,* **341,** 428–429.

——, and A. C. Dilley, 1981: Remote sounding of high clouds. IV: Observed temperature variations in cirrus optical properties. *J. Atmos. Sci.,* **38,** 1069–1082.

Ramanathan, V., R. D. Cess, E. F. Harrison, P. Minnis, B. R. Barkstrom, E. Ahmad, and D. Hartmann, 1989: Cloud-radiative forcing and climate: Results from the Earth Radiation Budget Experiment. *Science,* **243,** 57–63.

Remer, L. A., and Y. J. Kaufman, 2006: Aerosol direct radiative effect at the top of the atmosphere over cloud free ocean derived from four years of MODIS data. *Atmos. Chem. Phys.,* **6,** 237–253.

Roca, R., and V. Ramanathan, 2000: Scale dependence of monsoonal convective systems over the Indian Ocean. *J. Climate,* **13,** 1286–1298.

Rosenfeld, D., and I. M. Lensky, 1998: Satellite based insights into precipitation formation processes in continental and maritime convective clouds. *Bull. Amer. Meteor. Soc.,* **79,** 2457–2476.

——, and W. L. Woodley, 2000: Deep convective clouds with sustained supercooled liquid water down to −37.5°C. *Nature,* **405,** 440–442.

Rossow, W. B., and R. A. Schiffer, 1999: Advances in understanding clouds from ISCCP. *Bull. Amer. Meteor. Soc.,* **80,** 2261–2287.

Sherwood, S., 2002: A microphysical connection among biomass burning, cumulus clouds, and stratospheric moisture. *Science,* **295,** 1272–1275.

Stephens, G. L., 2005: Cloud feedbacks in the climate system: A critical review. *J. Climate,* **18,** 237–273.

——, S.-C. Tsay, P. W. Stackhouse Jr., and P. J. Flatau, 1990: The relevance of the microphysical and radiative properties of cirrus clouds to climate and climate feedback. *J. Atmos. Sci.,* **47,** 1742–1753.

Van Zadelhoff, G., E. Van Meijgaard, D. P. Donovan, W. H. Knap, and R. Boers, 2007: Sensitivity of the shortwave radiative budget to the parameterization of ice crystal effective radius. *J. Geophys. Res.,* **112,** D08213, doi:10.1029/2006JD007791.

Williams, E., and N. Renno, 1993: An analysis of the conditional instability of the tropical atmosphere. *Mon. Wea. Rev.,* **121,** 21–36.

Wyser, K., 1998: The effective radius in ice clouds. *J. Climate,* **11,** 1793–1802.

Xiong, X., J. Sun, and W. Barnes, 2008: Inter-comparison of on-orbit calibration consistency between Terra and Aqua MODIS reflective solar bands using the moon. *IEEE Geosci. Remote Sens. Lett.,* **5,** 778–782.

Xu, K.-M., T. Wong, B. A. Wielicki, D. A. Randall, L. Parker, and Z. A. Eitzen, 2005: Statistical analyses of satellite cloud object data from CERES. Part I: Methodology and preliminary results of the 1998 El Niño/2000 La Niña. *J. Climate,* **18,** 2497–2514.

——, ——, ——, L. Parker, B. Lin, Z. A. Eitzen, and M. Branson, 2007: Statistical analyses of satellite cloud object data from CERES. Part II: Tropical convective cloud objects during 1998 El Niño and validation of the fixed anvil temperature hypothesis. *J. Climate,* **20,** 819–842.

Yang, P., L. Zhang, G. Hong, S. L. Nasiri, B. A. Baum, H. Huang, M. D. King, and S. Platnick, 2007: Differences between collection 4 and 5 MODIS ice cloud optical/microphysical products and their impact on radiative forcing simulations. *IEEE Trans. Geosci. Remote Sens.,* **45,** 2886–2899, doi:10.1109/TGRS.2007.898276.

Yang, S., and E. A. Smith, 2006: Mechanisms for diurnal variability of global tropical rainfall observed from TRMM. *J. Climate,* **19,** 5190–5226.

Zipser, E. J., D. J. Cecil, C. Liu, S. W. Nesbitt, and D. P. Yorty, 2006: Where are the most intense thunderstorms on earth? *Bull. Amer. Meteor. Soc.,* **87,** 1057–1071.

Zurovac-Jevtic, D., and G. J. Zhang, 2003: Development and test of a cirrus parameterization scheme using NCAR CCM3. *J. Atmos. Sci.,* **60,** 1325–1344.